EUROPEAN ORGANIZATION FOR NUCLEAR RESEARCH

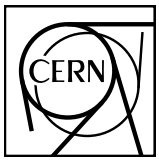

CERN-EP-2020-104
09 June 2020

A Triangle Singularity as the Origin of the $a_1(1420)$

The COMPASS Collaboration

Abstract

The COMPASS experiment recently discovered a new isovector resonance-like signal with axial-vector quantum numbers, the $a_1(1420)$, decaying to $f_0(980)\pi$. With a mass too close to and a width smaller than the axial-vector ground state $a_1(1260)$, it was immediately interpreted as a new light exotic meson, similar to the X, Y, Z states in the hidden-charm sector. We show that a resonance-like signal fully matching the experimental data is produced by the decay of the $a_1(1260)$ ground state into $K^*(K\pi)\bar{K}$ and subsequent rescattering through a triangle singularity into the coupled $f_0(980)\pi$ channel. The amplitude for this process is calculated using a novel method based on partial-wave projections. For the first time, the triangle singularity model is fitted to the partial-wave data of the COMPASS experiment. Despite having less parameters, this fit shows a slightly better quality than the one using a resonance hypothesis and thus eliminates the need for an additional resonance in order to describe the data. We thereby demonstrate for the first time that a resonance-like structure in the experimental data can be described by rescattering through a triangle singularity, providing evidence for a genuine three-body effect.

(to be submitted to PRL)

The COMPASS Collaboration

M.G. Alexeev[25,26], G.D. Alexeev[7], A. Amoroso[25,26], V. Andrieux[9,28], V. Anosov[7], A. Antoshkin[7], K. Augsten[7,18], W. Augustyniak[29], C.D.R. Azevedo[1], B. Badełek[30], F. Balestra[25,26], M. Ball[3], J. Barth[3], R. Beck[3], Y. Bedfer[20], J. Berenguer Antequera[25,26], J. Bernhard[12,9], M. Bodlak[17], F. Bradamante[24], A. Bressan[23,24], V. E. Burtsev[27], W.-C. Chang[21], C. Chatterjee[23,24], M. Chiosso[25,26], A. G. Chumakov[27], S.-U. Chung[15,a,b] A. Cicuttin[24,c] P. M. M. Correia[1], M.L. Crespo[24,c], D. D'Ago[23,24], S. Dalla Torre[24], S.S. Dasgupta[6], S. Dasgupta[24], I. Denisenko[7], O.Yu. Denisov[26,#], , S.V. Donskov[19], N. Doshita[32], Ch. Dreisbach[15], W. Dünnweber[d], R. R. Dusaev[27], A. Efremov[7], P.D. Eversheim[3], P. Faccioli[11], M. Faessler[d], M. Finger[17], M. Finger jr.[17], H. Fischer[8], C. Franco[11], J.M. Friedrich[15], V. Frolov[7,9], F. Gautheron[2,28], O.P. Gavrichtchouk[7], S. Gerassimov[14,15], J. Giarra[12], I. Gnesi[25,26], M. Gorzellik[8,e], A. Grasso[25,26], A. Gridin[7], M. Grosse Perdekamp[28], B. Grube[15], A. Guskov[7], D. von Harrach[12], R. Heitz[28], F. Herrmann[8], N. Horikawa[16,f], N. d'Hose[20], C.-Y. Hsieh[21,g], S. Huber[15], S. Ishimoto[32,h], A. Ivanov[7], T. Iwata[32], M. Jandek[18], V. Jary[18], R. Joosten[3], P. Jörg[8,i], E. Kabuß[12], F. Kaspar[15], A. Kerbizi[23,24], B. Ketzer[3], G.V. Khaustov[19], Yu.A. Khokhlov[19,j],Yu. Kisselev[7], F. Klein[4], J.H. Koivuniemi[2,28], V.N. Kolosov[19], K. Kondo Horikawa[32], I. Konorov[14,15], V.F. Konstantinov[19], A.M. Kotzinian[26,k], O.M. Kouznetsov[7], A. Koval[29], Z. Kral[17], F. Krinner[15], Y. Kulinich[28], F. Kunne[20], K. Kurek[29], R.P. Kurjata[31], A. Kveton[17], K. Lavickova[17], S. Levorato[24], Y.-S. Lian[21,l], J. Lichtenstadt[22], P.-J. Lin[20,m], R. Longo[28], V. E. Lyubovitskij[27,n], A. Maggiora[26], A. Magnon[o], N. Makins[28], N. Makke[24,c], G.K. Mallot[9,8], A. Maltsev[7], S. A. Mamon[27], B. Marianski[29], A. Martin[23,24], J. Marzec[31], J. Matoušek[23,24], T. Matsuda[13], G. Mattson[28], G.V. Meshcheryakov[7], M. Meyer[28,20], W. Meyer[2], Yu.V. Mikhailov[19], M. Mikhasenko[3,9,#], , E. Mitrofanov[7], N. Mitrofanov[7], Y. Miyachi[32], A. Moretti[23,24], A. Nagaytsev[7], C. Naim[20], D. Neyret[20], J. Nový[18], W.-D. Nowak[12], G. Nukazuka[32], A.S. Nunes[11,p], A.G. Olshevsky[7], M. Ostrick[12], D. Panzieri[26,q], B. Parsamyan[25,26], S. Paul[15], H. Pekeler[3], J.-C. Peng[28], M. Pešek[17], D.V. Peshekhonov[7], M. Pešková[17], N. Pierre[12,20], S. Platchkov[20], J. Pochodzalla[12], V.A. Polyakov[19], J. Pretz[4,s], M. Quaresma[21,11], C. Quintans[11], G. Reicherz[2], C. Riedl[28], T. Rudnicki[30], D.I. Ryabchikov[19,15], A. Rybnikov[7], A. Rychter[31], V.D. Samoylenko[19], A. Sandacz[29], S. Sarkar[6], I.A. Savin[7], G. Sbrizzai[23,24], H. Schmieden[4], A. Selyunin[7], L. Sinha[6], M. Slunecka[7,17], J. Smolik[7], A. Srnka[5], D. Steffen[9,15], M. Stolarski[11], O. Subrt[9,18], M. Sulc[10], H. Suzuki[32,f], P. Sznajder[29], S. Tessaro[24], F. Tessarotto[24,9,#], , A. Thiel[3], J. Tomsa[17], F. Tosello[26], A. Townsend[28], V. Tskhay[14], S. Uhl[15], B. I. Vasilishin[27], A. Vauth[4,9,r], B. M. Veit[12,9], J. Veloso[1], B. Ventura[20], A. Vidon[20], M. Virius[18], M. Wagner[3,#], , S. Wallner[15], K. Zaremba[31], P. Zavada[7], M. Zavertyaev[14], M. Zemko[17], E. Zemlyanichkina[7], Y. Zhao[24] and M. Ziembicki[31]

[1] University of Aveiro, Dept. of Physics, 3810-193 Aveiro, Portugal
[2] Universität Bochum, Institut für Experimentalphysik, 44780 Bochum, Germany[t,u]
[3] Universität Bonn, Helmholtz-Institut für Strahlen- und Kernphysik, 53115 Bonn, Germany[t]
[4] Universität Bonn, Physikalisches Institut, 53115 Bonn, Germany[t]
[5] Institute of Scientific Instruments of the CAS, 61264 Brno, Czech Republic[v]
[6] Matrivani Institute of Experimental Research & Education, Calcutta-700 030, India[w]
[7] Joint Institute for Nuclear Research, 141980 Dubna, Moscow region, Russia[x]
[8] Universität Freiburg, Physikalisches Institut, 79104 Freiburg, Germany[t,u]
[9] CERN, 1211 Geneva 23, Switzerland
[10] Technical University in Liberec, 46117 Liberec, Czech Republic[v]
[11] LIP, 1649-003 Lisbon, Portugal[y]
[12] Universität Mainz, Institut für Kernphysik, 55099 Mainz, Germany[t]
[13] University of Miyazaki, Miyazaki 889-2192, Japan[z]
[14] Lebedev Physical Institute, 119991 Moscow, Russia
[15] Technische Universität München, Physik Dept., 85748 Garching, Germany[t]
[16] Nagoya University, 464 Nagoya, Japan[z]

[17] Charles University, Faculty of Mathematics and Physics, 12116 Prague, Czech Republic[v]
[18] Czech Technical University in Prague, 16636 Prague, Czech Republic[v]
[19] State Scientific Center Institute for High Energy Physics of National Research Center 'Kurchatov Institute', 142281 Protvino, Russia
[20] IRFU, CEA, Université Paris-Saclay, 91191 Gif-sur-Yvette, France[u]
[21] Academia Sinica, Institute of Physics, Taipei 11529, Taiwan[aa]
[22] Tel Aviv University, School of Physics and Astronomy, 69978 Tel Aviv, Israel[ab]
[23] University of Trieste, Dept. of Physics, 34127 Trieste, Italy
[24] Trieste Section of INFN, 34127 Trieste, Italy
[25] University of Turin, Dept. of Physics, 10125 Turin, Italy
[26] Torino Section of INFN, 10125 Turin, Italy
[27] Tomsk Polytechnic University, 634050 Tomsk, Russia[ac]
[28] University of Illinois at Urbana-Champaign, Dept. of Physics, Urbana, IL 61801-3080, USA[ad]
[29] National Centre for Nuclear Research, 02-093 Warsaw, Poland[ae]
[30] University of Warsaw, Faculty of Physics, 02-093 Warsaw, Poland[ae]
[31] Warsaw University of Technology, Institute of Radioelectronics, 00-665 Warsaw, Poland[ae]
[32] Yamagata University, Yamagata 992-8510, Japan[z]

[#] Corresponding authors
[a] Also at Dept. of Physics, Pusan National University, Busan 609-735, Republic of Korea
[b] Also at Physics Dept., Brookhaven National Laboratory, Upton, NY 11973, USA
[c] Also at Abdus Salam ICTP, 34151 Trieste, Italy
[d] Supported by the DFG cluster of excellence 'Origin and Structure of the Universe' (www.universe-cluster.de) (Germany)
[e] Supported by the DFG Research Training Group Programmes 1102 and 2044 (Germany)
[f] Also at Chubu University, Kasugai, Aichi 487-8501, Japan
[g] Also at Dept. of Physics, National Central University, 300 Jhongda Road, Jhongli 32001, Taiwan
[h] Also at KEK, 1-1 Oho, Tsukuba, Ibaraki 305-0801, Japan
[i] Present address: Universität Bonn, Physikalisches Institut, 53115 Bonn, Germany
[j] Also at Moscow Institute of Physics and Technology, Moscow Region, 141700, Russia
[k] Also at Yerevan Physics Institute, Alikhanian Br. Street, Yerevan, Armenia, 0036
[l] Also at Dept. of Physics, National Kaohsiung Normal University, Kaohsiung County 824, Taiwan
[m] Supported by ANR, France with P2IO LabEx (ANR-10-LBX-0038) in the framework "Investissements d'Avenir" (ANR-11-IDEX-003-01)
[n] Also at Institut für Theoretische Physik, Universität Tübingen, 72076 Tübingen, Germany
[o] Retired
[p] Present address: Brookhaven National Laboratory, Brookhaven, USA
[q] Also at University of Eastern Piedmont, 15100 Alessandria, Italy
[r] Present address: Universität Hamburg, 20146 Hamburg, Germany
[s] Present address: RWTH Aachen University, III. Physikalisches Institut, 52056 Aachen, Germany
[t] Supported by BMBF - Bundesministerium für Bildung und Forschung (Germany)
[u] Supported by FP7, HadronPhysics3, Grant 283286 (European Union)
[v] Supported by MEYS, Grant LM20150581 (Czech Republic)
[w] Supported by B. Sen fund (India)
[x] Supported by CERN-RFBR Grant 12-02-91500
[y] Supported by FCT, Grants CERN/FIS-PAR/0007/2017 and CERN/FIS-PAR/0022/2019 (Portugal)
[z] Supported by MEXT and JSPS, Grants 18002006, 20540299, 18540281 and 26247032, the Daiko and Yamada Foundations (Japan)
[aa] Supported by the Ministry of Science and Technology (Taiwan)
[ab] Supported by the Israel Academy of Sciences and Humanities (Israel)

[ac] Supported by the Russian Federation program “Nauka” (Contract No. 0.1764.GZB.2017) (Russia)
[ad] Supported by the National Science Foundation, Grant no. PHY-1506416 (USA)
[ae] Supported by NCN, Grant 2017/26/M/ST2/00498 (Poland)

Quantum Chromodynamics (QCD) is generally accepted as the fundamental quantum-field theory of the strong interaction, one of the four forces known in nature. How exactly the spectrum of bound states (hadrons) emerges from the underlying interaction between quarks and gluons is, however, not yet understood. The main difficulty is the rise of the strong coupling at the low energy scale relevant for hadrons, which makes the theory unsolvable with perturbative methods. The quark model is an approach that describes the properties of hadrons by effective degrees of freedom represented by constituent quarks; mesons are assumed to be bound states of quarks and antiquarks in an attractive potential with a linearly rising confining part [1, 2]. Although the quark model describes many of the observed mesons, it seems that the spectrum is notably richer: there is growing experimental evidence for bound states beyond the constituent-quark model. Such states are commonly called exotic [3–8]. In addition to mapping out the full spectrum predicted by models and, more recently, by lattice gauge theory [9], the search for such exotic states drives the current interest in hadron spectroscopy.

The study of single-diffractive reactions with a high-energy meson beam, as performed by the COMPASS experiment at the CERN SPS [10, 11], is a natural way to investigate meson excitations (for a recent review, see Ref. [12]). In such reactions, at high energies commonly described by the exchange of a Pomeron $I\!P$, the incoming beam particle is excited by the strong interaction with a proton target. Regge theory then allows us to factorize off the target vertex, such that we only consider the beam vertex. Although the produced excited system immediately decays, the reaction products unveil the properties of the excitation. An unprecedented amount of data comprising almost 50 million events for the reaction $\pi^- + p \to \pi^-\pi^-\pi^+ + p$ was used by COMPASS to perform a detailed analysis of π_J and a_J mesons with isospin $I = 1$ and G-parity $G = -1$. The Partial-Wave Analysis (PWA) technique in connection with the isobar model was used to separate excitations with different quantum numbers, see Ref. [12, 13] for details. Individual waves are labeled $J^{PC} M^{\varepsilon}\, \xi\, \pi\, L$, where J is the total angular momentum of the 3-pion system, P the spatial and C the charge-conjugation parity. Note that although the charged states studied here are not eigenstates of the C operator, they are commonly labelled with the C-parity of the neutral member of the corresponding isospin multiplet, as inferred from $G = C(-1)^I$. The quantum number M labels the projection of the spin J onto the direction of the beam in the rest frame of $\pi^-\pi^-\pi^+$, and ε indicates the reflection symmetry with respect to the production plane. At the high center-of-momentum energies of the experiment, the reflectivity quantum number ε corresponds to the naturality of the exchanged particle and is hence always positive for Pomeron exchange. The orbital angular momentum between the neutral system of two pions (isobar) and the remaining pion is denoted by L. The symbol ξ labels the assumed isobar, *i.e.* the interaction amplitude in the neutral $\pi\pi$-subchannel.

A PWA including 88 waves in total was performed separately in 100 bins of the 3π invariant mass $m_{3\pi}$ and 11 bins of the reduced 4-momentum transfer squared t' [13]. The results are summarized in Fig. 1(a), where we show the intensities of selected waves as a function of $m_{3\pi}$, summed over all t' bins. Among many important observations, an exotic resonance-like signal with quantum numbers $J^{PC} = 1^{++}$ was found in the $1^{++}\,0^+\, f_0\pi\, P$-wave as a clear peak at $1.4\,\mathrm{GeV}/c^2$ [14] (see inset of Fig. 1(a)). The resonance-like behavior was corroborated by the observed phase motion, *i.e.* a mass-dependent relative phase with respect to several other reference waves. Extensive studies, also using the "freed-isobar" method [15], undoubtedly confirmed the signal and proved that it was not an artefact of any particular isobar parameterization [13]. In previous experiments, the resonance content of this wave was never analyzed because of its very small contribution. Following the PDG convention, the signal was called $a_1(1420)$ according to its quantum numbers $I^G(J^{PC}) = 1^-(1^{++})$. It was immediately realized that it could not be an ordinary quark-model meson resonance: (i) with about $150\,\mathrm{MeV}/c^2$, its width is much smaller than the width of the axial-vector ground state $a_1(1260)$ of about $500\,\mathrm{MeV}/c^2$; (ii) the signal is separated from the ground state by only about $150\,\mathrm{MeV}/c^2$, whereas the energy difference between different radial excitation levels is typically $400\,\mathrm{MeV}/c^2$ as estimated based on the slope of the radial excitation trajectory [16]; (iii) so far, the $a_1(1420)$ has been seen only in the $f_0(980)\pi$ final state.

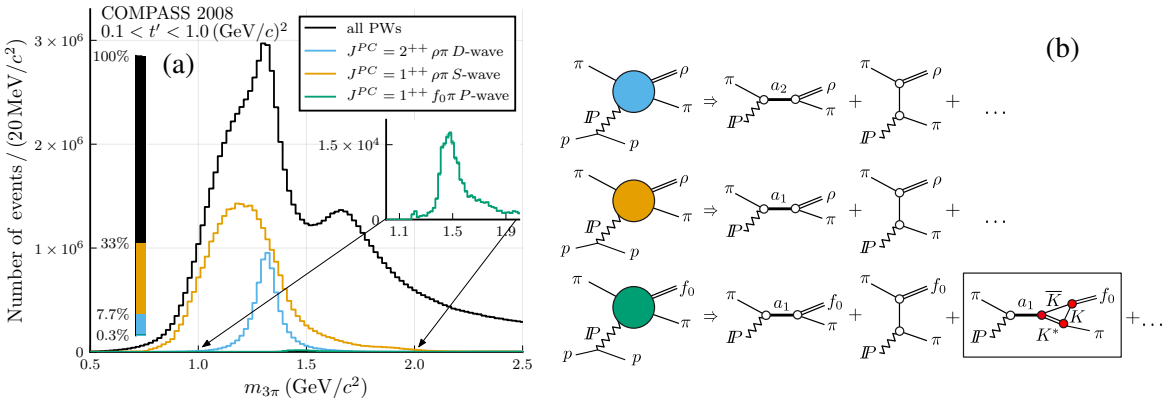

Fig. 1: (a) Intensities of selected waves from the PWA of the reaction $\pi^- + p \to \pi^-\pi^-\pi^+ + p$ [13]. The inset shows a zoomed view of the $1^{++}0^+\,f_0\pi P$-wave. The colored bar on the left indicates the contributions of the different waves to the total intensity. (b) Diagrams showing possible contributions to the $\rho(770)\pi$ and $f_0(980)\pi$ production amplitudes. The Pomeron is labelled $I\!P$, a_1 refers to the axial-vector ground state $a_1(1260)$, and a_2 to the tensor ground state $a_2(1320)$. The framed diagram shows the dominant contribution to the $a_1(1420)$ signal via the triangle diagram, as discussed in the present paper.

Various interpretations followed the $a_1(1420)$ observation [17–21]. They either do or do not require a new resonance. Resonances are consistently introduced in general scattering theory [22], where the reaction amplitude is an analytic function of the total energy squared s that is regarded as a complex number; they are found as poles on the unphysical sheet of the complex s-plane attached to the real axis from below. In explanations involving either diquark-antidiquark molecules or tightly bound tetraquarks, the observed signal, *i.e.* peak and phase motion, is caused by a pole-type singularity located on the closest sheet. Alternatively, a so-called triangle singularity [22, 23] was proposed as mechanism behind the $a_1(1420)$ signal [17]. Here, a logarithmic branch point caused by a coupled-channel effect, particularly by the $K^*\bar{K}$-$f_0\pi$ interaction, is located near the physical region on the closest unphysical sheet. A test of this interpretation is the subject of the present paper. For completeness, we mention an alternative model [21, 24] that does not require a new resonance pole, but instead combines resonant and non-resonant production mechanisms. The latter were shown in the past [25, 26] to be responsible for a large fraction of the reaction rate. In this model, the amplitude is made consistent with the requirement of probability conservation, *i.e.* unitarity of the scattering matrix. Applying it to the 1^{++} sector in COMPASS kinematics, a peak in the $1^{++}\,0^+\,f_0\pi P$-wave can be produced by specific adjustment of the relative production strengths between the $1^{++}0^+\,\rho\pi S$ and the $1^{++}\,0^+\,f_0\pi P$-waves. However, the generated phase motion between these waves at the position of the $a_1(1260)$ resonance is inconsistent with observation.

In the following, we briefly introduce the Triangle Singularity (TS) model and present a new method for the calculation of the amplitude, which goes beyond Ref. [17] and in principle allows us to include also higher-order rescattering effects. The full details of the calculation will be published in a forthcoming paper.

The dynamics of a hadronic three-body system is commonly understood in terms of quasi two-body interactions with subchannel resonances ξ decaying further into pairs of final-state particles. Often, however, the same final state can be obtained through several decay chains when the two-particle interaction is non-negligible for different particle pairs [27, 28]. Different decay chains are coherent, hence they interfere. Moreover, the unitarity of the scattering matrix enforces a consistency relation between the different chains [29–31]. This relation makes the lineshape of the two-particle resonances in a system of three particles dependent on the dynamics in the other pair [32–35]. An equivalent way of describing this interrelation between pair-wise interactions is to state that the cross-channel two-body resonances in the $\pi\pi$, $K\pi$ and $\bar{K}K$ systems rescatter to one another, thereby modifying the original undistorted line-

shapes. In the particular case considered in this paper, the dominant cross-channel resonances involved are $K^*(892)$ and $f_0(980)$. In addition to affecting the lineshapes, the probabilities for a three-body resonance decaying to one or another channel may be redistributed due to final-state interaction [36, 37]. This effect is strongly enhanced for certain kinematic conditions [22, 38] and produces the observed resonance-like signal (TS) in the case considered here.

We find that the presence of the $K^*(892)$ resonance (hereafter referred to as K^*) in the $K\bar{K}\pi$ channel drastically affects the $f_0(980)\pi$ channel, since the rescattering between $K^* \to K\pi P$-wave and $K\bar{K} \to f_0(980) \to \pi\pi S$-wave occurs with all intermediate particles being almost on their mass shell for $m_{3\pi} \approx 1.4\,\mathrm{GeV}/c^2$, *i.e.* slightly above the $K^*\bar{K}$ threshold [17]. This effect does not disturb the narrow lineshape of the $f_0(980)$, but it leads to a significant redistribution of the $a_1(1260)$ decay probabilities. The originally negligible $f_0(980)\pi P$-wave decay channel is populated by the rescattering from the $K^*\bar{K}$ decay locally around $1.4\,\mathrm{GeV}/c^2$.

For the calculation of the TS amplitude we use a novel partial-wave-projection method based on the requirement of unitarity applied to the partial-wave projection of the three-body transition amplitude [39]. This leads us to the Khuri-Treiman equation [29–31] for the production amplitude $F_W^{\{1\}}$ of a three-particle system (123) with a given set of quantum numbers W, invariant mass squared $s \equiv m_{3\pi}^2$, and the isobar formed by particles 2 and 3 (hereafter labelled $\{1\}$ using circular indices) with invariant mass squared $\sigma_{\{1\}} \equiv (p_2+p_3)^2$:

$$F_W^{\{1\}}(s,\sigma_{\{1\}}) = C_W^{\{1\}}(s) + \sum_\omega \frac{K_W^{\{1\}}(s,\sigma_{\{1\}})}{2\pi} \int_{\sigma_{\mathrm{th},W}}^{\infty} \frac{\rho(\sigma)\hat{F}_{W,\omega}^{\{1\}}(s,\sigma)}{K_W^{\{1\}}(s,\sigma)(\sigma-\sigma_{\{1\}}-i\varepsilon)}\mathrm{d}\sigma. \tag{1}$$

Here, the indices W and ω refer to the full set of quantum numbers labeling a given wave. For the $f_0\pi P$-wave considered in this paper, $K_W^{\{1\}}(s,\sigma_{\{1\}})$ is a kinematic-singularity factor equal to the $f_0\pi$ break-up momentum in the center-of-momentum frame. The term $C_W^{\{1\}}(s)$ parameterizes the three-body production dynamics and the decay into the given final state W. It includes the direct production of the $a_1(1260)$ resonance and a term for the non-resonant production that is further described below. The sum runs over all possible cross channels with quantum numbers ω. In the dispersion integral, $\rho(\sigma)$ is the 2-body phase-space factor, and $\hat{F}_{W,\omega}^{\{1\}}(s,\sigma)$ is the projection of the cross channel $\{3\}$, i.e. the isobar formed by particles 1 and 2, with quantum numbers ω onto channel $\{1\}$ with quantum numbers W. We do not expect isobars in channel $\{2\}$, formed by *e.g.* $K^-\pi^-$, $K^0\pi^-$ or $\pi^-\pi^-$. Figure 2 shows the $m_{3\pi}$ dependence of the $f_0(980)\pi$ isobar production amplitude for different individual cross channels ω. The blue lines represent the TS in the $K\bar{K}\pi$ channel with the K^* resonance. The full blue line is the result of the new partial-wave projection method, Eq. (1), taking into account the spins of all particles involved. The dashed blue line labeled "(scalar)", as well as all other dashed lines, are obtained by calculations using the Feynman method from Ref. [17], neglecting the spins of the involved particles. The curves shown in dashed gray correspond to the rescattering effects of the various $\pi\pi$ resonances in the cross channel. For the calculation we assume that modifications of the lineshapes of the cross-channel resonances due to rescattering are negligible. It can be seen that the $K^*\bar{K}$ channel produces a narrow peak and a strong phase motion at the mass of the $a_1(1420)$ due to the TS being very close to the physical region, while all other channels including the direct decay and the non-resonant background (Bgd) manifest themselves in a broad bump and a slow phase motion.

In order to perform a fit of the TS model to the COMPASS spin-density matrix elements (SDMEs) [41], we choose the three waves depicted in Fig. 1(b), which constitute the dominant contributions to the $\rho\pi$ and $f_0\pi$ production amplitudes: (i) the $1^{++}0^+\,\rho\pi S$-wave describes the source of the rescattering process, since its largest contribution comes from the $a_1(1260)$. This wave also contains a significant contribution from non-resonant "Deck"-like processes [26]; (ii) the $1^{++}0^+\,f_0\pi P$-wave contains the $a_1(1420)$ signal;

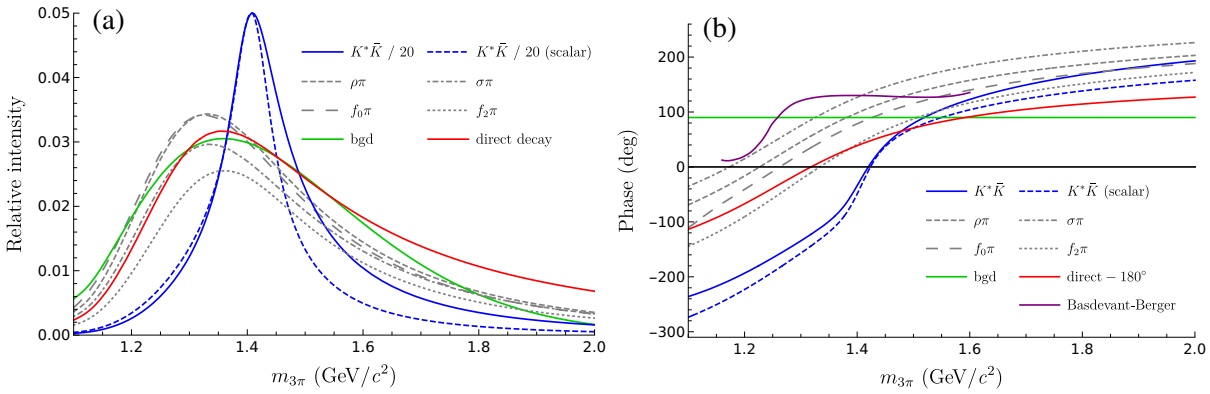

Fig. 2: (a) Intensities and (b) phases of the $f_0\pi P$ amplitude produced from different sources. The $m_{3\pi}$ dependence is shown for the $f_0(980)$ subchannel invariant mass fixed to the nominal resonance mass of 990 MeV/c^2. See text and Refs. [13, 40] for details on the calculations and the descriptions of the parameterizations of the isobar and resonance amplitudes. The intensities in panel (a) are relative to the maximum intensity of the $K^*\bar{K}$ channel, with the couplings in each vertex set to unity. Note that the intensity of the $K^*\bar{K}$ triangle graph (blue lines) was scaled down by a factor of 20. In panel (b) we also include the phase from Ref. [21] (purple line). Its inflection point is at a mass of approximately 1.25 GeV/c^2. See text for details on the different curves.

(iii) the $2^{++}1^+\,\rho\pi D$-wave exhibits a clean $a_2(1320)$-resonance and is included in order to fix the relative phases and stabilize the fit. In general, there are two components for each wave in the model: a resonance amplitude, *i.e.* a propagator that contains a pole (in this case either the $a_1(1260)$ or the $a_2(1320)$), and a component with t-channel π exchange accounting for non-resonant processes. We parameterize the $a_1(1260)$ propagator by a relativistic Breit-Wigner amplitude with energy-dependent width saturated by the $\rho\pi$ decay channel [40]. For the resonance part of the $\rho\pi D$-wave we employ the $a_2(1320)$ propagator parameterized by a Breit-Wigner amplitude with dynamical width including the $\rho\pi$ (80%) and $\eta\pi$ (20%) channels, as discussed in Ref. [40]. The non-resonant background is added coherently to each wave. We use an empirical parameterization given by $(m_{3\pi}/m_0 - 1)^b \exp[-(c_0 + c_1 t' + c_2 t'^2)\tilde{p}^2]$, where $\tilde{p}$ is an effective break-up momentum for the decay into $\xi\pi$ at the given $m_{3\pi}$ value, taking into account the finite width of the isobar ξ and the Bose symmetry of the system, and $m_0 = 0.5\,\text{GeV}/c^2$ (see Eq. (27) in Ref. [40]). For the model calculations, the t' value is fixed to the lower edge of the respective bin. For the $f_0\pi P$-wave, the resonance part of the production amplitude is modified by the $K^*\bar{K} \to f_0\pi$-rescattering via the TS. As the direct decay of the $a_1(1260)$ to the $f_0\pi$ final state has a very slow phase motion and a similar shape as the phenomenological parameterization of the non-resonant part (compare the red and green curves in Fig. 2), the fit cannot distinguish between the two components. The direct decay of the $a_1(1260)$ to $f_0\pi$ is hence omitted.

The free parameters of the model, *i.e.* the t'-dependent complex couplings, the background parameters b and c_i, as well as the t'-independent Breit-Wigner resonance parameters, are determined by a fit to the results of the PWA in $m_{3\pi}$ and t' bins. We note that the TS amplitude is parameter-free. As explained in more detail in Ref. [40], the data points y_i to be fitted are the intensity and the real and imaginary parts of the interference terms for the 3 selected waves inside the chosen $m_{3\pi}$ ranges (indicated in Fig. 3) for all 11 t' bins. The fit is performed by minimizing the sum of the squared differences between data points y_i (SDMEs) and model prediction $\hat{y}_i$, weighted by the inverse squared statistical uncertainties:

$$\mathscr{R}^2 = \sum_i \frac{(y_i - \hat{y}_i)^2}{\sigma_i^2}. \tag{2}$$

Since not all of the data points used in the fit are independent quantities, the quantity $\mathscr{R}^2$ is not a strict χ^2; its use is nevertheless advantageous, since all waves enter the $\mathscr{R}^2$ function in a symmetric manner.

Figure 3 shows the result of the TS model fit in the lowest t' bin, selecting only the $f_0\pi P$-wave (full

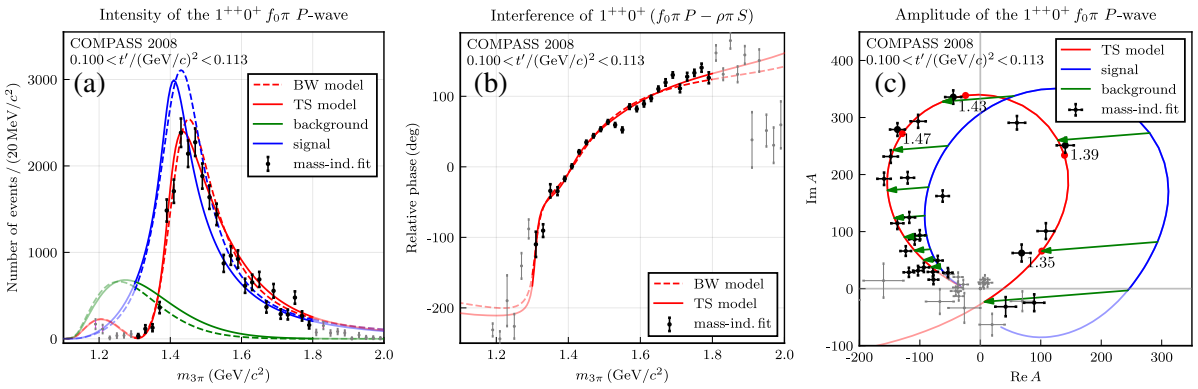

Fig. 3: Results of the fit with the TS model (solid lines) and the Breit-Wigner model (dashed lines) to the wave with the $a_1(1420)$ resonance-like signal. The fit range is indicated by the color saturation of data points and lines. (a) intensity of the $1^{++}0^+ f_0\pi P$-wave. The complete fit model (red) is decomposed into its signal (blue) and background (green) contributions. (b) relative phase between the $1^{++}0^+ \rho\pi S$-wave and the $1^{++}0^+ f_0\pi P$-wave. Since our simple background model has a constant phase, we omit the separation of signal and background contributions. (c) Argand diagram. The red dots on the TS-model curve correspond to the indicated $m_{3\pi}$ values in units of GeV/c^2.

lines). The fit results for all three waves in all 11 t'-bins can be found in Ref. [42]. Panel (a) shows the intensity of the $f_0\pi P$-wave and panel (b) the relative phase to the $\rho\pi S$-wave, both as a function of $m_{3\pi}$. The resonance-like behavior of the TS amplitude is most evident from the circle in the Argand diagram in panel (c). The non-resonant background (green arrows) helps to slightly adjust the position of the circle. Since the phase of the background component does not change with $m_{3\pi}$, all green arrows are parallel.

In order to evaluate the quality of the TS model fit, we also perform a fit to the data using a simple Breit-Wigner description of the $a_1(1420)$ signal instead of the TS amplitude. This is accomplished by replacing the TS parameterization of the $f_0\pi P$-wave by a relativistic Breit-Wigner amplitude with free mass and width parameters assuming the $a_1(1420)$ being a genuine new resonance. We use a constant-width parameterization since further decay modes of this hypothetical new particle are unknown. Figure 3 shows that the fits with the Breit-Wigner model (dashed) and the TS model (solid) are of very similar quality. Both models are capable of describing the intensities as well as the corresponding interference terms. The advantage of the TS model is that it has two fit parameters less, since it does not require a new particle with corresponding mass and width. For a quantitative comparison, one can use a quantity defined in analogy to Eq. (2). The biggest contribution comes from the $\rho\pi S$ and $\rho\pi D$-waves. Since the description of these two waves is very similar in both fit models, we can omit them for the comparison of the fit quality. In addition, we can exclude one of the two remaining phases of the interferences, since they depend linearly on one another. Defining $\mathscr{R}^2_{\mathrm{red}}$ as the reduced weighted sum of the remaining residuals squared divided by the number of degrees of freedom, where only the fit parameters specific to the $f_0\pi P$-wave are taken into account, we arrive at a value of $\mathscr{R}^2_{\mathrm{red,TS}} = 4.8$ for the TS and $\mathscr{R}^2_{\mathrm{red,BW}} = 5.2$ for the Breit-Wigner model, suggesting a slightly better description of the $a_1(1420)$ signal by the TS model.

In order to study the stability of the result, we investigate a wide range of sources of systematic uncertainties, both with respect to changes of the model and to changes of the data points (SDMEs). We perform fits where the data points y_i are varied according to systematic studies for the PWA in bins of mass and t', published in Ref. [13]. These include using a smaller wave set, removing negative reflectivity waves, relaxing the event selection, using rank 2 instead of rank 1, or changing the parameterization of the $f_0(980)$. In an additional study, we use the result of a statistical re-analysis of [13] applying the bootstrap technique [43]. Also, we consider several variations in the fit model for the TS: (i) a

fit with non-Bose-symmetrized phase space; (ii) neglecting the spins of the particles involved (similar to Ref. [17]); and (iii) including the excitations $a_1(1640)$ and $a_2(1700)$ in the $\rho\pi S$ and $\rho\pi D$ waves, respectively (mass and width fixed to the values from the PDG [1]). We see that the TS model systematically yields a slightly smaller $\mathscr{R}^2_{\text{red}}$ than the Breit-Wigner model [42].

In summary, we have shown that the recently discovered resonance-like signal with axial-vector quantum numbers, the $a_1(1420)$ observed by COMPASS in the decay to $f_0(980)\pi$, can be fully explained by the decay of the ground-state $a_1(1260)$ into $K^*\bar{K}$ and subsequent rescattering through a triangle singularity into $f_0(980)\pi$. To our knowledge, this is the first time that a rescattering model is fitted successfully to experimental data, mimicking a resonance-like signal. It appears that the fit quality of the TS model in terms of $\mathscr{R}^2_{\text{red}}$ is even slightly better than that of the Breit-Wigner model, also throughout almost all our systematic studies. This result suggests that there is no need for the existence of a new genuine a_1 resonance in order to describe the data. The effect due to rescattering via the Triangle Singularity, which is expected to be present, is sufficient to explain the observation.

Acknowledgments.—We gratefully acknowledge the support of the CERN management and staff as well as the skills and efforts of the technicians of our collaborating institutions. We would like to thank Bastian Kubis for useful discussions on the scalar form-factor. This work was made possible by the financial support of our funding agencies: MEYS Grant No. LG13031 (Czech Republic); FP7 "HadronPhysics3" Grant No. 283286 (European Union); CEA, P2I and ANR (France); BMBF Collaborative Research Project 05P2018 - COMPASS, DFG Cluster of Excellence "Origin and Structure of the Universe", DFG Research Training Group Programmes 1102 and 2044 (Germany); B. Sen Fund (India); Academy of Sciences and Humanities (Israel); INFN (Italy); MEXT and JSPS, Grants No. 8002006, No. 20540299, and No. 18540281, Daiko and Yamada Foundations (Japan); NCN Grant No. 2017/26/M/ST2/00498 (Poland); FCT Grants No. CERN/FIS-PAR/0007/2017 and CERN/FIS-PAR/0022/ 2019 (Portugal); CERN-RFBR Grant No. 12-02-91500, Presidential Grant No. NSh-999.2014.2 (Russia); MST (Taiwan); and NSF (USA).

References

[1] M. Tanabashi, et al., Review of Particle Physics, Phys. Rev. D98 (3) (2018) 030001. doi:10.1103/PhysRevD.98.030001.

[2] D. Ebert, R. N. Faustov, V. O. Galkin, Mass spectra and Regge trajectories of light mesons in the relativistic quark model, Phys. Rev. D79 (2009) 114029. arXiv:0903.5183, doi:10.1103/PhysRevD.79.114029.

[3] B. Ketzer, Hybrid Mesons, PoS QNP2012 (2012) 025. arXiv:1208.5125.

[4] C. A. Meyer, E. S. Swanson, Hybrid Mesons, Prog. Part. Nucl. Phys. 82 (2015) 21–58. arXiv:1502.07276, doi:10.1016/j.ppnp.2015.03.001.

[5] A. Esposito, A. Pilloni, A. D. Polosa, Multiquark Resonances, Phys. Rept. 668 (2017) 1–97. arXiv:1611.07920, doi:10.1016/j.physrep.2016.11.002.

[6] F.-K. Guo, C. Hanhart, U.-G. Meissner, Q. Wang, Q. Zhao, B.-S. Zou, Hadronic molecules, Rev. Mod. Phys. 90 (1) (2018) 015004. arXiv:1705.00141, doi:10.1103/RevModPhys.90.015004.

[7] S. L. Olsen, T. Skwarnicki, D. Zieminska, Nonstandard heavy mesons and baryons: Experimental evidence, Rev. Mod. Phys. 90 (1) (2018) 015003. arXiv:1708.04012, doi:10.1103/RevModPhys.90.015003.

[8] A. Rodas, et al., Determination of the pole position of the lightest hybrid meson candidate, Phys. Rev. Lett. 122 (4) (2019) 042002. arXiv:1810.04171, doi:10.1103/PhysRevLett.122.042002.

[9] J. J. Dudek, R. G. Edwards, P. Guo, C. E. Thomas, Toward the excited isoscalar meson spectrum

from lattice QCD, Phys. Rev. D88 (9) (2013) 094505. arXiv:1309.2608, doi:10.1103/PhysRevD.88.094505.

[10] P. Abbon, et al., The COMPASS experiment at CERN, Nucl. Instr. Meth. A 577 (2007) 455–518. arXiv:hep-ex/0703049.

[11] P. Abbon, et al., The COMPASS Setup for Physics with Hadron Beams, Nucl. Instr. Meth. A 779 (2015) 69–115. arXiv:1410.1797, doi:10.1016/j.nima.2015.01.035.

[12] B. Ketzer, B. Grube, D. Ryabchikov, Light-Meson Spectroscopy with COMPASS, Progress in Particle and Nuclear Physics, in press (2020) 103755. arXiv:1909.06366, doi:https://doi.org/10.1016/j.ppnp.2020.103755.
URL http://www.sciencedirect.com/science/article/pii/S0146641020300028

[13] C. Adolph, et al., Resonance Production and $\pi\pi$ S-wave in $\pi^- + p \to \pi^-\pi^-\pi^+ + p_{\text{recoil}}$ at 190 GeV/c, Phys. Rev. D 95 (2017) 032004. arXiv:1509.00992, doi:10.1103/PhysRevD.95.032004.

[14] C. Adolph, et al., Observation of a New Narrow Axial-Vector Meson $a_1(1420)$, Phys. Rev. Lett. 115 (8) (2015) 082001. arXiv:1501.05732, doi:10.1103/PhysRevLett.115.082001.

[15] F. Krinner, D. Greenwald, D. Ryabchikov, B. Grube, S. Paul, Ambiguities in model-independent partial-wave analysis, Phys. Rev. D 97 (2018) 114008. arXiv:1710.09849, doi:10.1103/PhysRevD.97.114008.

[16] K. Chen, C.-Q. Pang, X. Liu, T. Matsuki, Light axial vector mesons, Phys. Rev. D91 (7) (2015) 074025. arXiv:1501.07766, doi:10.1103/PhysRevD.91.074025.

[17] M. Mikhasenko, B. Ketzer, A. Sarantsev, Nature of the $a_1(1420)$, Phys. Rev. D 91 (2015) 094015. arXiv:1501.07023, doi:10.1103/PhysRevD.91.094015.

[18] F. Aceti, L. R. Dai, E. Oset, $a_1(1420)$ peak as the $\pi f_0(980)$ decay mode of the $a_1(1260)$, Phys. Rev. D94 (9) (2016) 096015. arXiv:1606.06893, doi:10.1103/PhysRevD.94.096015.

[19] H.-X. Chen, E.-L. Cui, W. Chen, T. G. Steele, X. Liu, S.-L. Zhu, $a_1(1420)$ resonance as a tetraquark state and its isospin partner, Phys. Rev. D91 (2015) 094022. arXiv:1503.02597, doi:10.1103/PhysRevD.91.094022.

[20] T. Gutsche, M. A. Ivanov, J. G. Körner, V. E. Lyubovitskij, K. Xu, Test of the multiquark structure of $a_1(1420)$ in strong two-body decays, Phys. Rev. D 96 (11) (2017) 114004. arXiv:1710.02357, doi:10.1103/PhysRevD.96.114004.

[21] J.-L. Basdevant, E. L. Berger, Peak locations and relative phase of different decay modes of the a_1 axial vector resonance in diffractive production, Phys. Rev. Lett. 114 (19) (2015) 192001. arXiv:1504.05955, doi:10.1103/PhysRevLett.114.192001.

[22] V. N. Gribov, Y. L. Dokshitzer, J. Nyiri, Strong Interactions of Hadrons at High Energies – Gribov Lectures on Theoretical Physics, Cambridge University Press, Cambridge, 2009.

[23] R. Eden, Regge poles and elementary particles, Rept. Prog. Phys. 34 (1971) 995–1053. doi:10.1088/0034-4885/34/3/304.

[24] J.-L. Basdevant, E. L. Berger, Unitary Coupled-Channel Analysis of Diffractive Production of the a1 Resonance, Phys. Rev. D16 (1977) 657. doi:10.1103/PhysRevD.16.657.

[25] R. T. Deck, Kinematical interpretation of the first pi - rho resonance, Phys. Rev. Lett. 13 (1964) 169–173. doi:10.1103/PhysRevLett.13.169.

[26] G. Ascoli, L. M. Jones, B. Weinstein, H. W. Wyld, Partial-wave analysis of the deck amplitude for $\pi N \to \pi\pi\pi N^*$, Phys. Rev. D 8 (1973) 3894–3919. doi:10.1103/PhysRevD.8.3894.

[27] D. Herndon, P. Soding, R. J. Cashmore, A GENERALIZED ISOBAR MODEL FORMALISM, Phys. Rev. D11 (1975) 3165. doi:10.1103/PhysRevD.11.3165.

[28] I. J. R. Aitchison, Dispersion Theory Model of Three-Body Production and Decay Processes, Phys. Rev. 137 (1965) B1070–B1084. doi:10.1103/PhysRev.137.B1070.

[29] N. N. Khuri, S. B. Treiman, Pion-Pion Scattering and $K^{\pm} \to 3\pi$ Decay, Phys. Rev. 119 (1960) 1115–1121. doi:10.1103/PhysRev.119.1115.

[30] R. Pasquier, J. Y. Pasquier, Khuri-Treiman-Type Equations for Three-Body Decay and Production Processes, Phys. Rev. 170 (1968) 1294–1309. doi:10.1103/PhysRev.170.1294.

[31] R. Pasquier, J. Y. Pasquier, Khuri-treiman-type equations for three-body decay and production processes. 2., Phys. Rev. 177 (1969) 2482–2493. doi:10.1103/PhysRev.177.2482.

[32] I. J. R. Aitchison, J. J. Brehm, ARE THERE IMPORTANT UNITARITY CORRECTIONS TO THE ISOBAR MODEL?, Phys. Lett. B 84 (1979) 349–353. doi:10.1016/0370-2693(79)90056-X.

[33] F. Niecknig, B. Kubis, Dispersion-theoretical analysis of the $D^+ \to K^-\pi^+\pi^+$ Dalitz plot, JHEP 10 (2015) 142. arXiv:1509.03188, doi:10.1007/JHEP10(2015)142.

[34] F. Niecknig, B. Kubis, S. P. Schneider, Dispersive analysis of $\omega \to 3\pi$ and $\phi \to 3\pi$ decays, Eur. Phys. J. C72 (2012) 2014. arXiv:1203.2501, doi:10.1140/epjc/s10052-012-2014-1.

[35] I. V. Danilkin, C. Fernandez-Ramirez, P. Guo, V. Mathieu, D. Schott, M. Shi, A. P. Szczepaniak, Dispersive analysis of $\omega/\phi \to 3\pi, \pi\gamma*$, Phys. Rev. D 91 (9) (2015) 094029. arXiv:1409.7708, doi:10.1103/PhysRevD.91.094029.

[36] C. Schmid, Final-State Interactions and the Simulation of Resonances, Phys. Rev. 154 (5) (1967) 1363. doi:10.1103/PhysRev.154.1363.

[37] A. P. Szczepaniak, Dalitz plot distributions in presence of triangle singularities, Phys. Lett. B757 (2016) 61–64. arXiv:1510.01789, doi:10.1016/j.physletb.2016.03.064.

[38] L. Landau, On analytic properties of vertex parts in quantum field theory, Nucl. Phys. 13 (1959) 181–192. doi:10.1016/0029-5582(59)90154-3.

[39] M. Mikhasenko, Three-pion dynamics at COMPASS: resonances, rescattering and non-resonant processes, Ph.D. thesis, Rheinische Friedrich-Wilhelms-Universität Bonn (2019).

[40] M. Aghasyan, et al., Light isovector resonances in $\pi^- p \to \pi^-\pi^-\pi^+ p$ at 190 GeV/c, Phys. Rev. D 98 (2018) 092003. arXiv:1802.05913, doi:10.1103/PhysRevD.98.092003.

[41] See data tables in HEPData repository at http://www.hepdata.net/record/82958.

[42] M. Aghasyan, et al., A Triangle Singularity as the Origin of the $a_1(1420)$—Supplemental Material, Suppl. Material for PRL.

[43] B. Efron, R. Tibshirani, An introduction to the bootstrap, Statist. Sci. 57 (1) (1986) 54–75.

Supplemental material

.1 Systematic studies

We investigate several sources of systematic uncertainties including variations of the fit model and uncertainties of the mass-independent PWA. We perform fits where the data points (SDMEs) y_i in Eq. (2) of the main text are varied according to systematic studies for the PWA in bins of mass and t' (see Ref. [13]). Figure .1 compares the quantity $\mathscr{R}^2_{\text{red}}$, as defined in Eq. (2), for the TS model and the model using a simple Breit-Wigner amplitude for the $a_1(1420)$, for the various studies. These include using a smaller wave set ("53 waves"), removing negative-reflectivity waves ("no neg. waves"), relaxing the event selection ("coarse ev. sel."), using rank 2 instead of rank 1 ("rank 2"), and changing the parameterization of the $f_0(980)$ ("$f_0(980)$ BW", "$(\pi\pi)_S\, K_1$"). In an additional study, we use the result of a statistical re-analysis of [13] applying the bootstrap technique [43] ("bootstrap"). Also, we consider several variations of the fit model for the TS: (i) a fit with non-Bose-symmetrized phase space ("non-sym. ph. sp."); (ii) neglecting the spins of the particles involved (similar to Ref. [17], "scalar TS"); and (iii) including the excitations $a_1(1640)$ and $a_2(1700)$ in the $\rho\pi S$ and $\rho\pi D$ waves, respectively (masses and widths fixed to the values from the PDG [1], "excited res."). We see from Fig. .1 that the TS model systematically yields a slightly smaller $\mathscr{R}^2_{\text{red}}$ than the Breit-Wigner model.

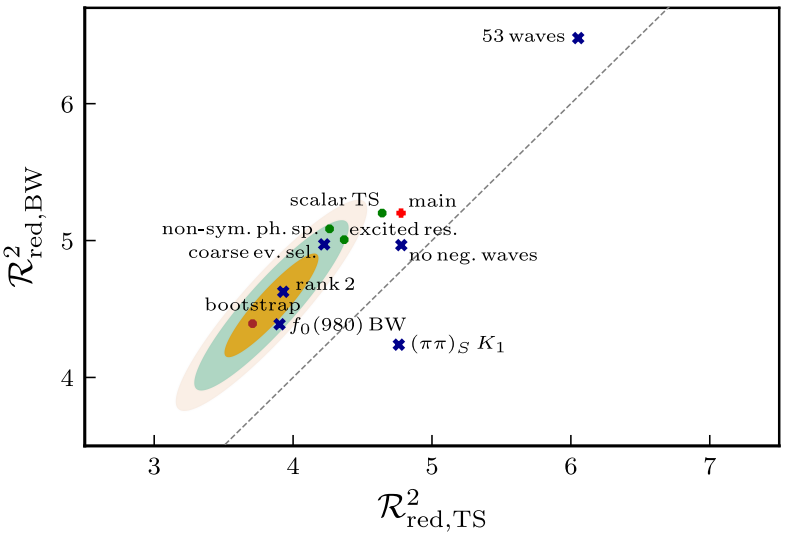

Fig. .1: $\mathscr{R}^2_{\text{red,BW}}$ for the Breit-Wigner model vs. $\mathscr{R}^2_{\text{red,TS}}$ for the TS model. See main text for details on their definition. The main fit shown in Fig. 3 is represented by the red cross, the gray dashed line indicates $\mathscr{R}^2_{\text{red,BW}} = \mathscr{R}^2_{\text{red,TS}}$. Blue crosses correspond to systematic studies using different data points and green dots show the fit results with a modified model of the $f_0\pi P$ wave. The result of the bootstrap analysis is shown by the filled ellipses which cover 68 %, 95 %, and 99 % of the obtained sample, respectively; the fit to the bootstrap-sample mean is represented by the brown point.

.2 Fit result for all t' bins

Figures .2 – .12 show the spin-density matrix elements (SDMEs) of the three waves selected for the model fit (data points) and the fit results of the TS model for all t'-bins. The full fit model (red) is decomposed into signal (blue) and background (green) as described in the main text. The intensities are plotted on the diagonal and the complex phase of the interference parts on the off-diagonal. The 3 rows as well as the 3 columns correspond to the $1^{++}0^{+}\rho\pi S$, $1^{++}0^{+}f_0\pi P$, and $2^{++}1^{+}\rho\pi D$-waves.

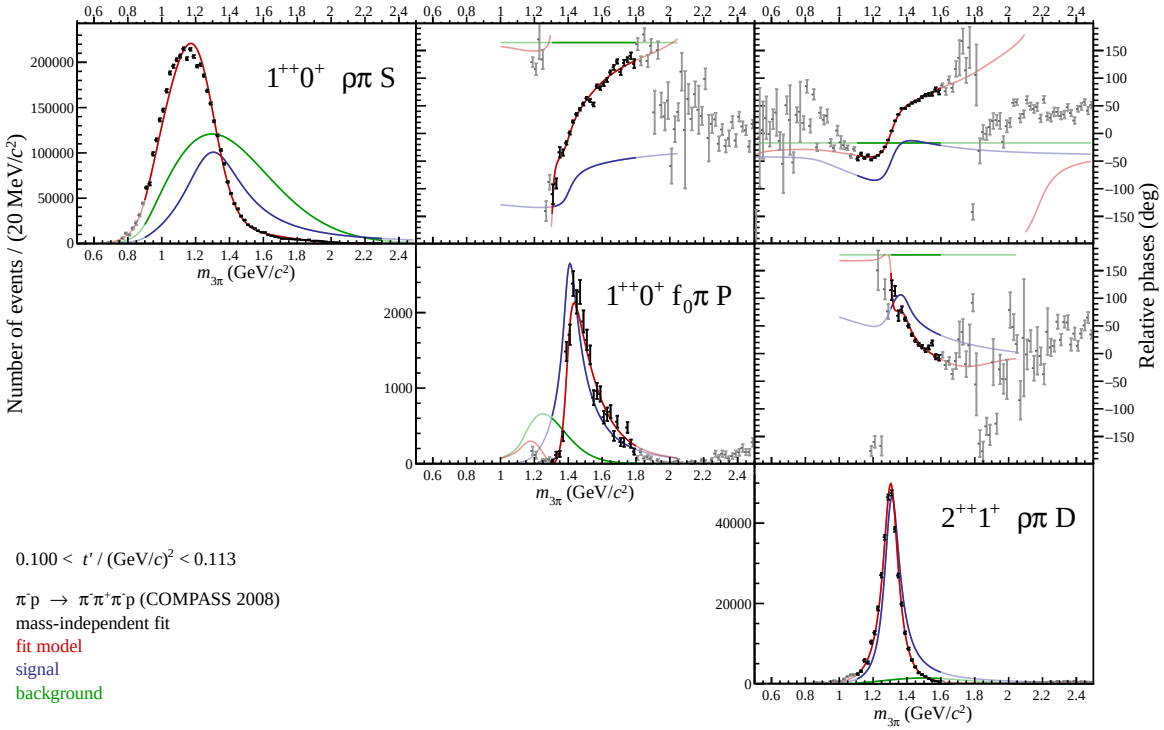

Fig. .2: Spin-density matrix elements of the 3 waves selected for the TS model fit and the corresponding fit results, both shown for the first (lowest) bin of t'. The SDMEs as a function of $m_{3\pi}$ are visualized in the form of a 3×3 upper-triangular matrix of graphs with the partial-wave intensities on the diagonal and the relative phases between the partial waves on the off-diagonal. Black crosses correspond to the result of the PWA in bins of $m_{3\pi}$ and t' from Ref. [13] with statistical uncertainties indicated by vertical lines. The data are overlaid by the TS model curve (red), the contributions from signal (blue) and non-resonant background (green). The $m_{3\pi}$ fit range is indicated by the color saturation of data points and fit result. Regions indicated by lower color saturation were not included in the fit; the model curves in these regions are extrapolations.

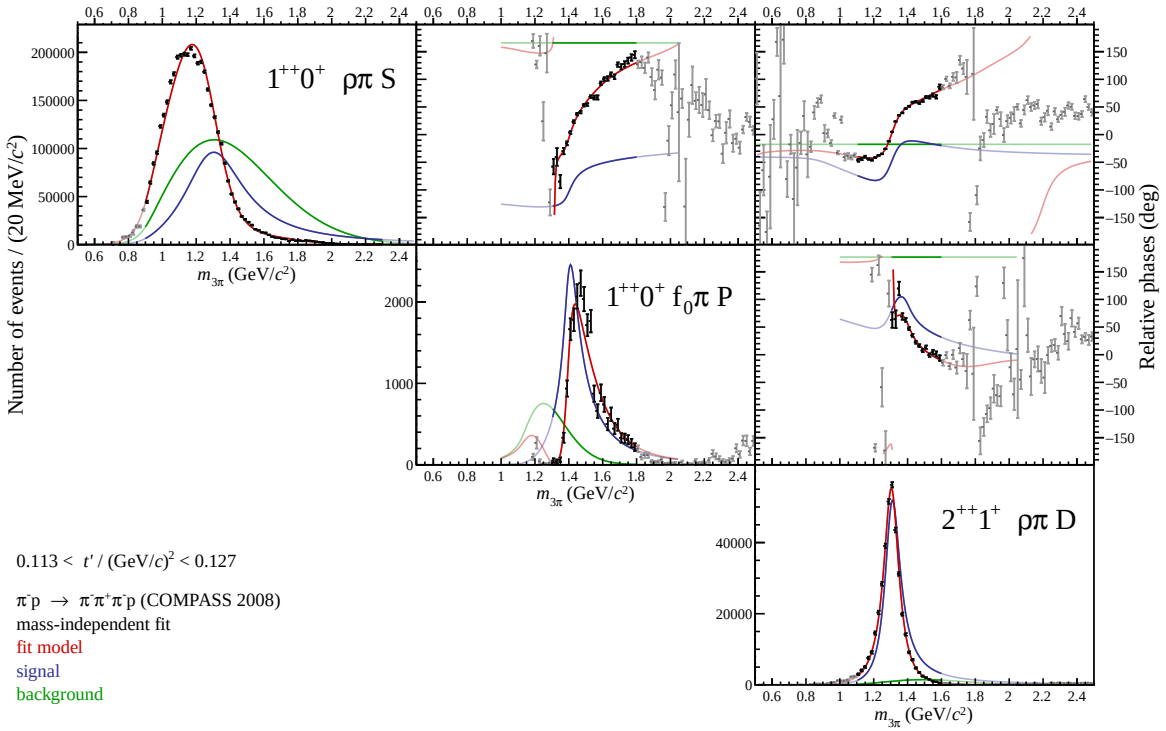

Fig. .3: Same as Fig. .2, but for t'-bin 2.

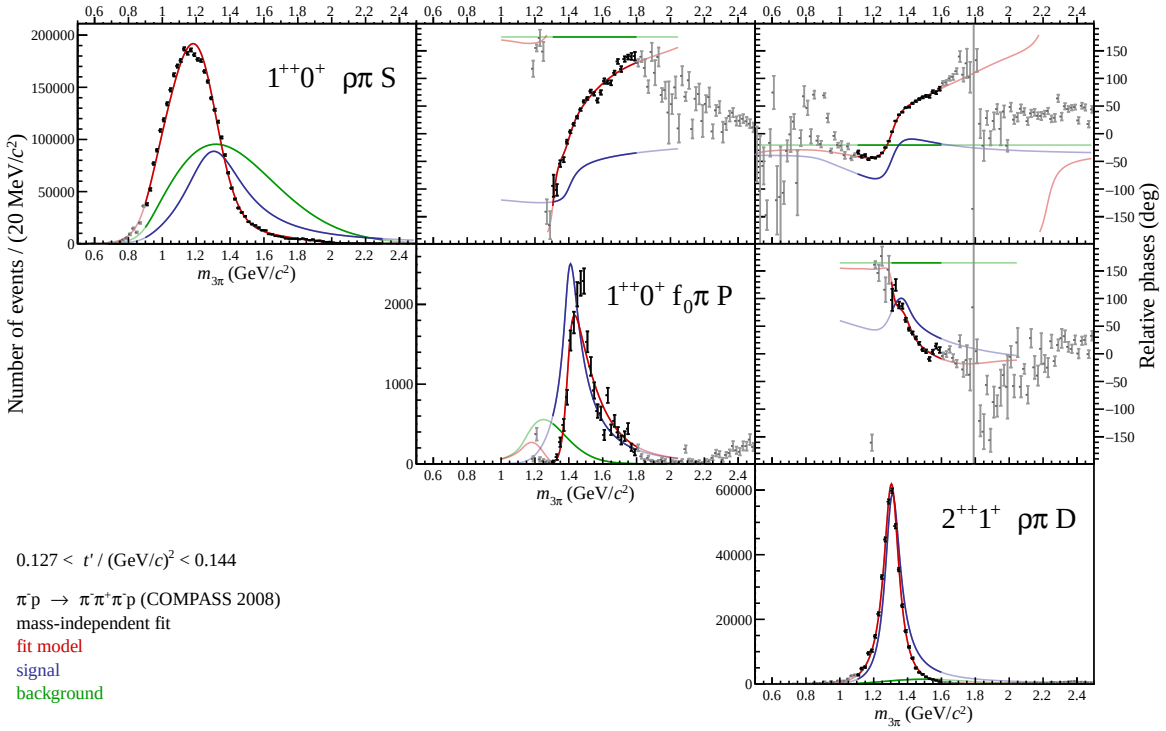

Fig. .4: Same as Fig. .2, but for t'-bin 3.

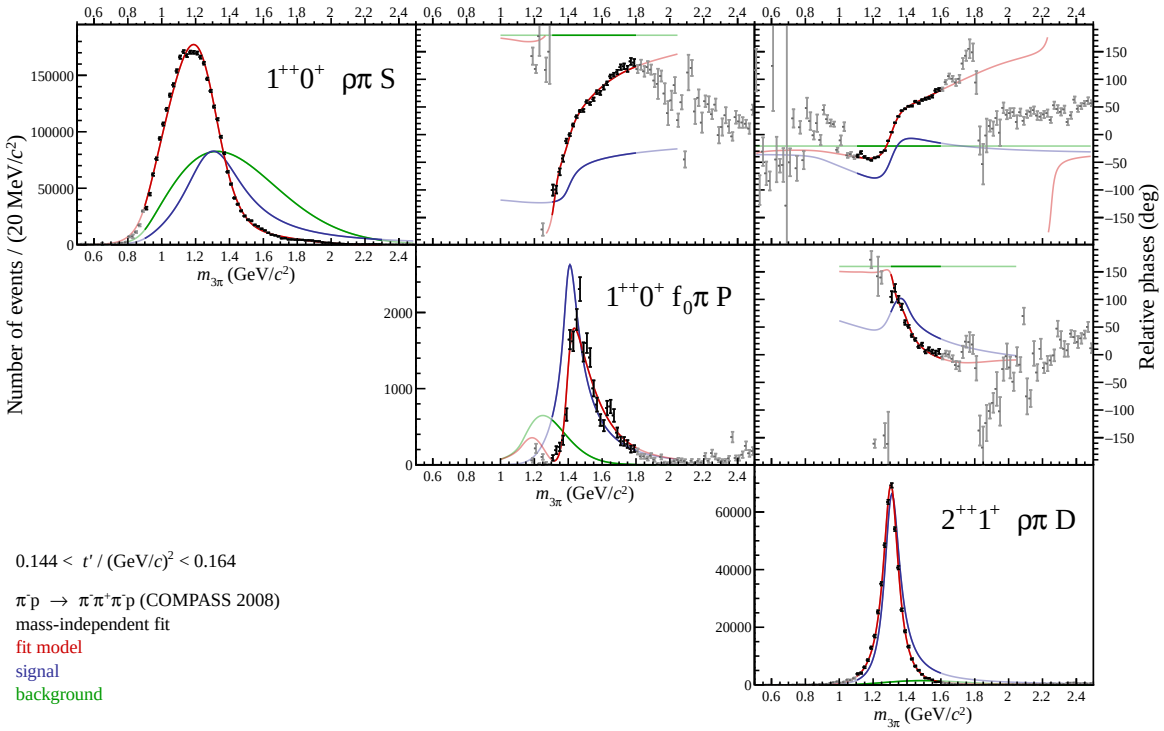

Fig. .5: Same as Fig. .2, but for t'-bin 4.

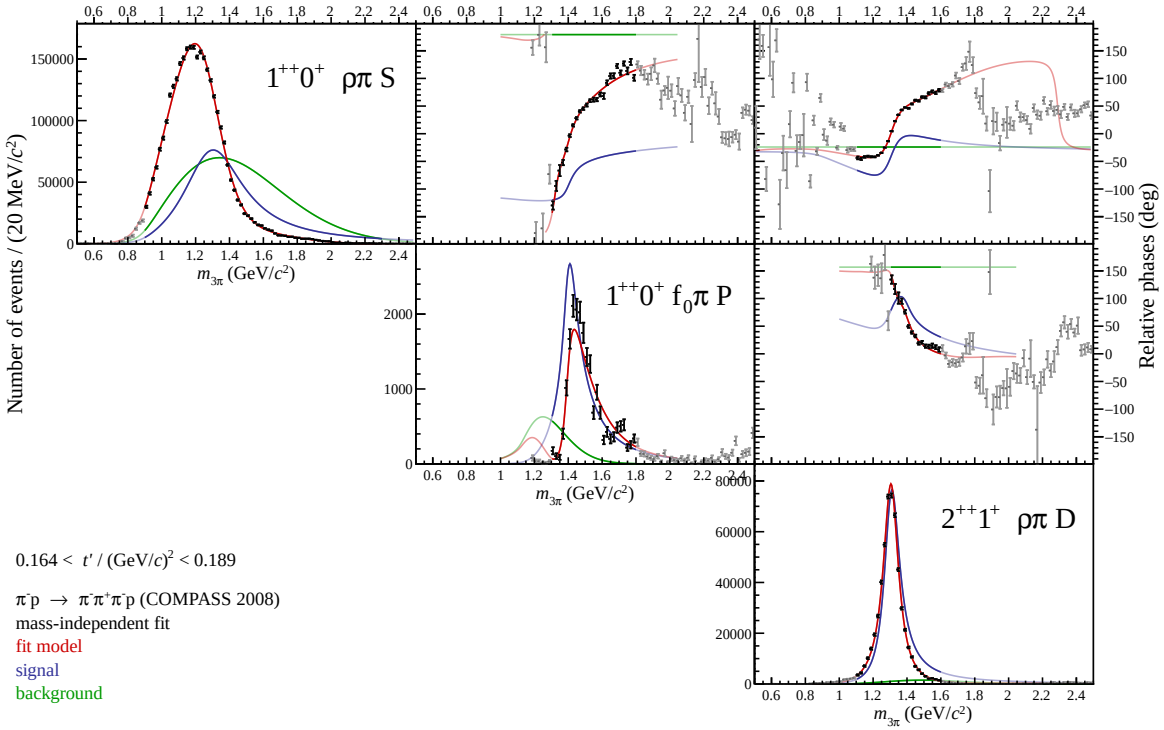

Fig. .6: Same as Fig. .2, but for t'-bin 5.

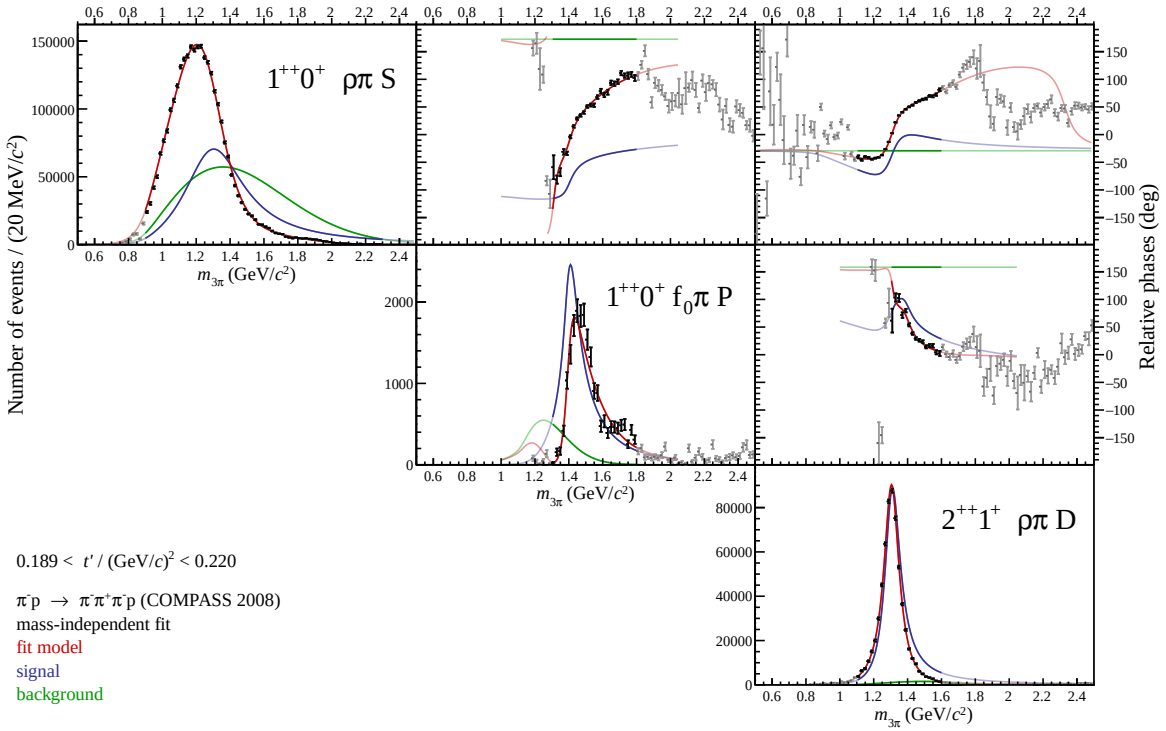

Fig. .7: Same as Fig. .2, but for t'-bin 6.

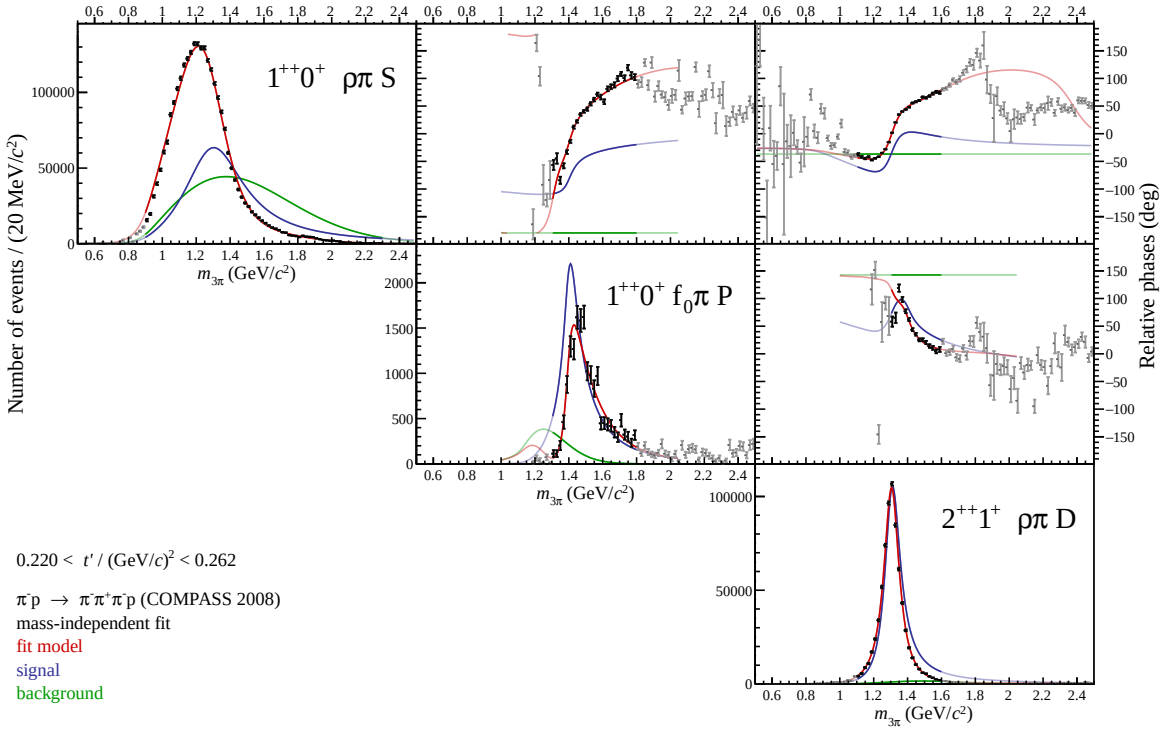

Fig. .8: Same as Fig. .2, but for t'-bin 7.

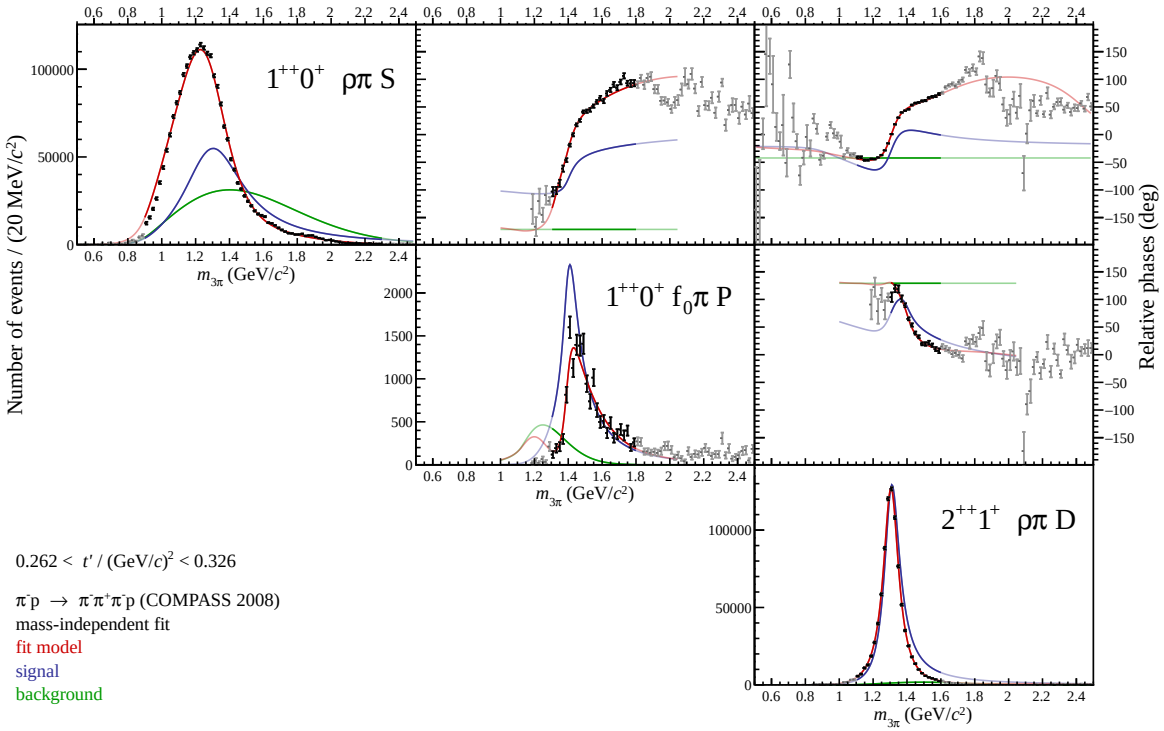

Fig. .9: Same as Fig. .2, but for t'-bin 8.

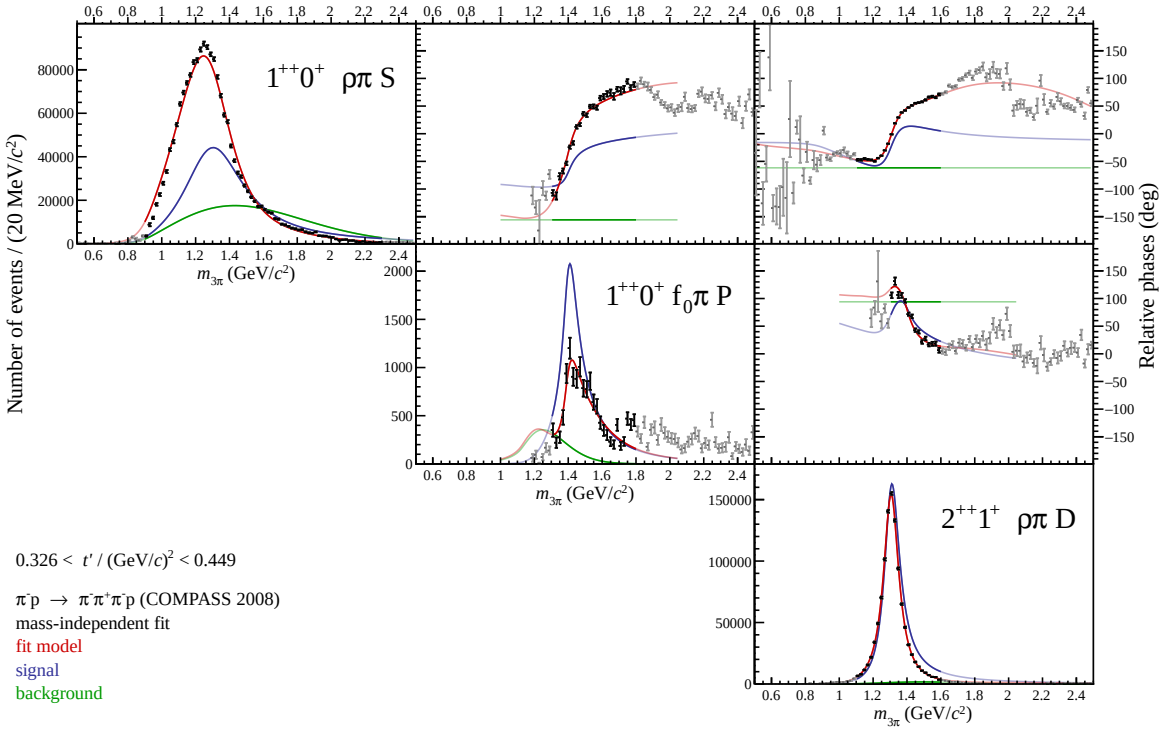

Fig. .10: Same as Fig. .2, but for t'-bin 9.

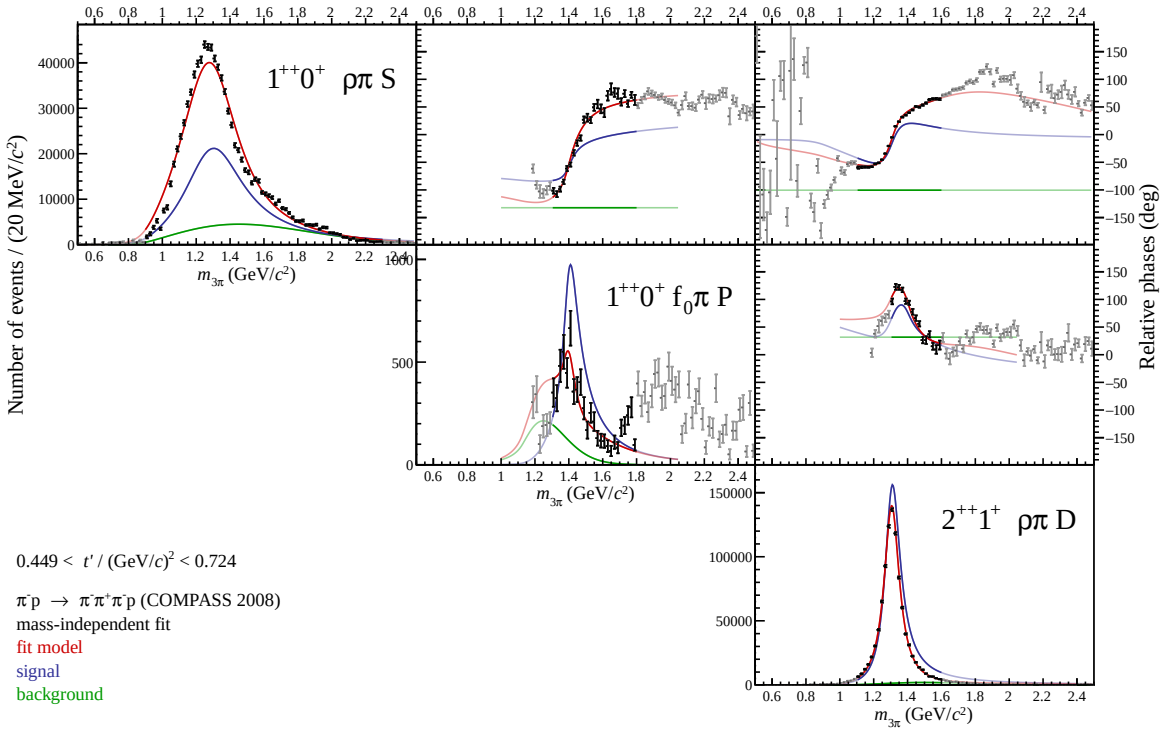

Fig. .11: Same as Fig. .2, but for t'-bin 10.

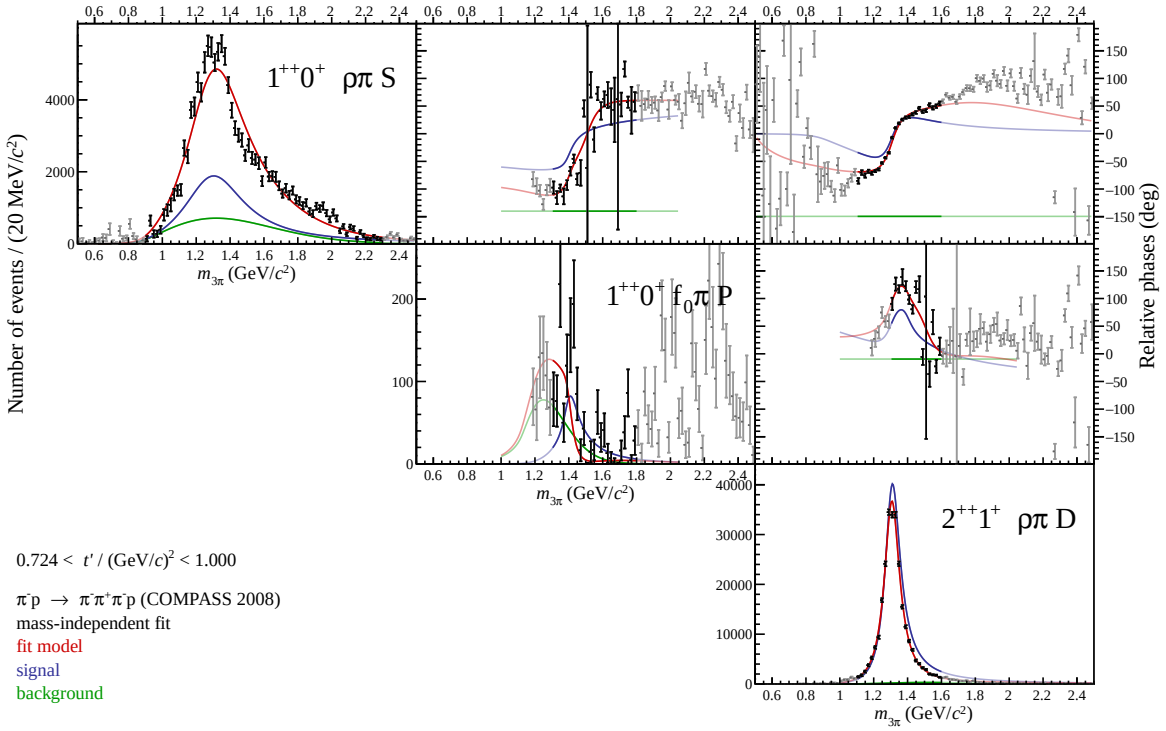

Fig. .12: Same as Fig. .2, but for t'-bin 11.